Geophysical Journal International

Geophys. J. Int. (2015) **203,** 1113–1127
GJI Seismology

doi: 10.1093/gji/ggv338

Seismic tomography reveals a mid-crustal intrusive body, fluid pathways and their relation to the earthquake swarms in West Bohemia/Vogtland

Sima Mousavi,[1] Klaus Bauer,[2] Michael Korn[1] and Babak Hejrani[3]

[1] *Institute of Geophysics and Geology, University of Leipzig, Talstr.* 35, *D*-4103 *Leipzig, Germany, E-mail: seyede_sima.mousavi@uni-leipzig.de*
[2] *GFZ German Research Centre for Geosciences, Telegrafenberg, D*-14473 *Potsdam, Germany*
[3] *Research School of Earth Sciences, Australian National University, Canberra, ACT, Australia*

Accepted 2015 August 14. Received 2015 July 28; in original form 2014 December 15

SUMMARY

The region of West Bohemia/Vogtland in the Czech–German border area is well known for the repeated occurrence of earthquake swarms, CO_2 emanations and mofette fields. We present a local earthquake tomography study undertaken to image the Vp and Vp/Vs structure in the broader area of earthquake swarm activity. In comparison with previous investigations, more details of the near-surface geology, potential fluid pathways and features around and below the swarm focal zone could be revealed. In the uppermost crust, for the first time the Cheb basin and the Bublák/Hartoušov mofette fields were imaged as distinct anomalies of Vp and Vp/Vs. The well-pronounced low-Vp anomaly of the Cheb basin is not continuing into the Eger rift indicating a particular role of the basin within the rift system. A steep channel of increased Vp/Vs is interpreted as the pathway for fluids ascending from the earthquake swarm focal zone up to the Bublák/Hartoušov mofette fields. As a new feature, a mid-crustal body of high Vp and increased Vp/Vs is revealed just below and north of the earthquake swarm focal zone. It may represent a solidified intrusive body which emplaced prior or during the formation of the rift system. We speculate that enhanced fluid flow into the focal zone and triggering of earthquakes could be driven by the presence of the intrusive body if cooling is not fully completed. We consider the assumed intrusive structure as a heterogeneity leading to higher stress particularly at the junction of the rift system with the basin and prominent fault structures. This may additionally contribute to the triggering of earthquakes.

Key words: Seismicity and tectonics; Body waves; Seismic tomography; Europe.

1 INTRODUCTION

The region of West Bohemia/Vogtland in the German–Czech border area is known for its complicated past and present geodynamical activities like repeated occurrence of earthquake swarms (e.g. Horálek & Fischer 2008), presence of mantle derived CO_2 and He isotopes, increased heat flow (Čermák *et al.* 1996), gas vents, mofettes, mineral waters, geothermal springs (Heinicke & Koch 2000; Weise *et al.* 2001), quaternary volcanoes (Wagner *et al.* 2002) and negative gravity anomaly (Švancara *et al.* 2000, 2008). These observations indicate a high potential of current and future dynamic activities. At present, there is no complete explanation for such a concentration of various geodynamical phenomena in this small area.

One of the most significant geodynamic features in West Bohemia is the periodical re-occurrence of earthquake swarms in an intracontinental region (Fischer *et al.* 2014). In general, earthquake swarms mainly occur in mid-ocean rifts and active volcanic areas which are related to magma and fluid movements and they are usually associated with degassing (e.g. Dreger *et al.* 2000). Similarly, for West Bohemia, ongoing magmatic processes and related transport of fluids and their interplay with tectonic structures can be assumed as the responsible scenario for the generation of seismicity. The geotectonic setting is determined by the post-Variscan structures of the Eger rift and the Cheb basin (Fig. 1). In fact, the swarm seismicity concentrates at the conjunction of the rift graben and the basin, where also prominent faults are running parallel to the seismic event distribution (e.g. Horálek *et al.* 1996; Bankwitz *et al.* 2003; Fischer *et al.* 2014). The possible role of fluids in the generation of earthquake swarms was early recognized by several authors (Weinlich *et al.* 1998; Heinicke & Koch 2000; Weise *et al.* 2001; Bräuer *et al.* 2005; Bräuer *et al.* 2009; Kämpf *et al.* 2013). Magmatic source regions for these fluids were suggested to be located within the deeper crust around the Moho (Špičak & Horálek 2001; Weise *et al.* 2001) and within the upper mantle (Bräuer *et al.* 2003; Hofmann *et al.* 2003; Geissler *et al.* 2005; Heuer *et al.* 2006; Heuer *et al.* 2011).

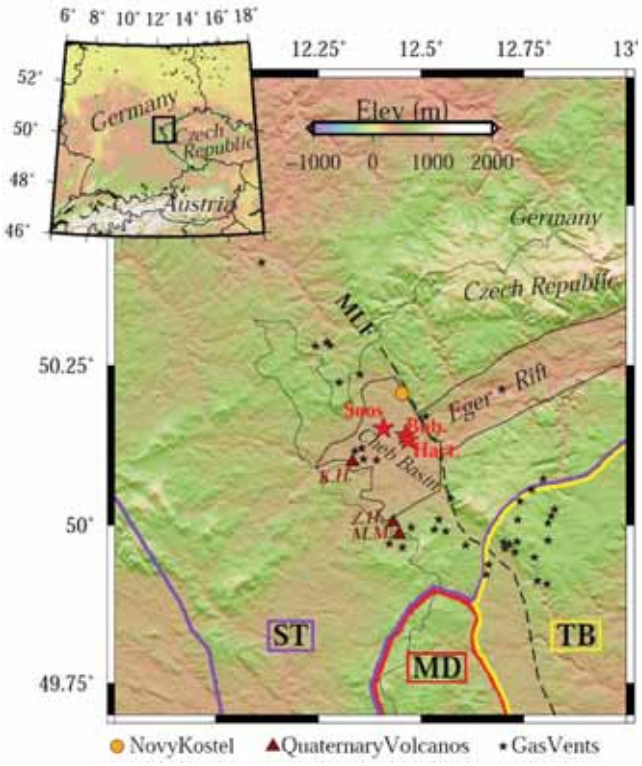

Figure 1. Topographic map of NW Bohemia and its location within Europe. The tectonic setting is determined by the microplates of the Saxothuringian (ST), Moldanubian (MD) and Teplá-Barandian (TB). The earthquake swarms are concentrating at the intersection between Eger rift, Cheb basin and Mariánské Lázně fault (MLF), close to the community of Nový Kostel. High rates of fluid and gas flow from deeper crustal and mantle sources are measured at mofettes and gas vents. Quaternary volcanoes are shown as red triangles: Komorní hůrka (KH), Železná hůrka (ZH) and Mýtina (MM). Main mofette fields inside Cheb basin including Hartoušov mofette (Hart.) and Bublák mofette (Bub.) and Soos are marked by red stars.

Many geophysical investigations were performed using different techniques to derive structural constraints on the proposed mechanisms for the unusual earthquake swarm behaviour. Overviews of such studies are given, for example, in Novotný *et al.* (2013) and Fischer *et al.* (2014). The method of local earthquake tomography (LET) provides information on the Vp and Vp/Vs crustal structure within the context of the seismicity distribution. Hence, LET is particularly suited to test the hypothesis that fluids originating from deeper magmatic sources play an important role in the swarm generation, and that the geochemical sampling of fluids at the surface provides a window into these crustal processes (e.g. Weise *et al.* 2001).

Recent LET studies delivered images of Vp, Vp/Vs and seismicity for West Bohemia using various data sets and different traveltime inversion techniques (Růžek & Horálek 2013; Alexandrakis *et al.* 2014). Růžek & Horálek (2013) derived for the first time smooth 3-D velocity models of the upper crust in West Bohemia from independent inversions for Vp and Vs. Alexandrakis *et al.* (2014) applied the double-difference tomography program TomoDD (Zhang & Thurber 2003) and determined relative perturbations of Vp, Vp/Vs anomalies and earthquake locations around the earthquake swarm region. Here we present a traveltime inversion for absolute values of Vp, Vp/Vs and seismicity distribution using the SIMUL2000 tomography package (Thurber 1983; Eberhart-Phillips 1993; Thurber 1993). In extension to the previous investigations of Růžek & Horálek (2013) and Alexandrakis *et al.* (2014), our tomography study is based on a larger distribution of seismological stations covering regions in the Czech Republic and in Germany. The results allow us for the first time to identify features such as the Cheb basin and fluid path ways between the earthquake swarm region and the Bublák/Hartoušov mofette fields (Fig. 1), as predicted from previous interpretations of surface geochemical data (e.g. Weise *et al.* 2001).

2 GEOLOGICAL AND TECTONIC SETTING

The Bohemian Massif is located considerably far away from existing plate boundaries and active volcanoes (Špičak & Horálek 2001). It was formed as a consequence of the complex Variscan orogeny which included ocean closure, accretion of terranes and continental collision, subduction, followed by a period of strike-slip faulting (Matte *et al.* 1990). The Bohemian Massif is subdivided into the Saxothuringian Zone, Moldanubian and Teplá-Barandian which differ in metamorphic grade and tectonic setting (e.g. Zulauf *et al.* 2002). The borders of these geotectonic domains are shown in Fig. 1.

Eger rift, quaternary volcanoes, Cheb basin and Mariánské Lázně fault (MLF) zone are the main post-Variscan geological features of West Bohemia (Fig. 1). The NE–SW striking Eger rift is part of the European Cenozoic rift system (Ziegler 1992). It was formed in response to the Alpidian orogeny and related far-field accumulations and release of stress along pre-existing Variscan structures. The graben development was lasting until the Late Miocene and the rift appears mostly inactive at present. The Cheb basin, the youngest geological feature in NW Bohemia, was formed in the late Tertiary and Quaternary. It developed at the junction of the Eger rift and MLF (Dudek 1986). Lithologies encountered within the basin include metamorphic crystalline rocks, granites and fluvial sediments (Kämpf *et al.* 2013). The Quaternary volcanoes Komorní hůrka and Železná hůrka and a recently discovered volcano Mýtina (Mrlina *et al.* 2009) are located along the western margin of the Cheb basin (Babuška *et al.* 2008).

The majority of earthquake swarm foci in West Bohemia are clustered close to the community of Nový Kostel, at the northeastern edge of the Cheb basin where it intersects the MLF and the Eger rift. The Nový Kostel focal zone is located at the top of the Variscan granite (Hecht *et al.* 1997). Earthquakes occur at the depth range between 6 and 11 km, with maximum magnitudes of $M_L < 4.6$. Recent swarm activities were observed in 2000, 2008, 2011 and 2014.

The source mechanism in swarm focal zone was studied by number of authors (e.g. Dahm *et al.* 2008; Hainzl *et al.* 2012; Horálek & Šílený 2013; Vavryčuk *et al.* 2013). The focal mechanisms are in general consistent with the stress field of the western European lithosphere with subhorizontal T axis in NE–SW direction. Additional to shear faulting there is evidence for volumetric source components pointing to faults that are under high fluid pressure exceeding the principal stresses.

Horálek *et al.* (1996) related earthquake swarms in West Bohemia to tectonic faults. A possible connection between earthquake activities and underground fluids in West Bohemia has been addressed for the first time by Weinlich *et al.* (1998). Later Špičak & Horálek (2001) suggested that the occurrence of earthquake swarms is associated with magmatic activity in the deeper crust. Kurz *et al.* (2003) estimated that the regional stress field is not strong enough

to cause earthquake swarms while pore pressure and temperature play an important role in the earthquake swarm generation. Kurz *et al.* (2004) linked the earthquake swarm occurrence to recent crustal magmatic activity and related fluids. Bräuer *et al.* (2003) and Hofmann *et al.* (2003) assumed an active magma reservoir in the upper mantle which is the source of upward fluid migration. Sampling and measurement of He isotopes indicated that the fluids released from gas vents and springs within and around the Cheb basin have a magmatic source (Bräuer *et al.* 2005). Weise *et al.* (2001) and Bräuer *et al.* (2009) suggested that earthquakes were triggered by mantle-derived magmatic fluids. Their hypothesis got supported by measurements on $^3He/^4He$ anomalies and CO_2 discharge in mofettes and mineral springs.

The lithospheric structure within the earthquake swarm region shows an updoming Moho and a low-velocity zone in the uppermost mantle based on receiver function studies (Geissler *et al.* 2005; Heuer *et al.* 2006). The low-velocity layer was identified at around 65 km depth and was interpreted as partial melts or an asthenospheric updoming (Heuer *et al.* 2006). A baby mantle plume was proposed by Heuer *et al.* (2011) based on weak depth variations of the 410-km discontinuity. The idea of a magmatic body around the mantle–crust transition was rejected by Plomerová *et al.* (2007), since they did not find any 'tube-like' low-velocity heterogeneity as a result of their teleseismic tomography investigation.

3 LOCAL EARTHQUAKE DATA

The data set for this study was generated based on recordings of permanent and temporary seismic networks in Germany and Czech Republic during the time period of 2000–2010. WEBNET and KRASNET—the permanent local seismic networks of the Czech Republic—have build up the main part of data in addition to permanent stations of BAYERNNETZ, SXNET and Thuringian network in Germany. Temporary networks BOHEMA (Plomerová *et al.* 2003), PASSEQ (Wilde-Piórko *et al.* 2008) and temporary networks of institutions such as GFZ, SZGRF, University of Potsdam and University of Freiberg were the other sources of our data set. Fig. 2 shows the distribution of stations used in this study.

Considering that swarms are concentrated within small hypocentral volumes and about 90 per cent of the recorded earthquakes are located near Nový Kostel, our initial catalogue contained many earthquakes from almost identical source locations. To avoid redundancy and unbalanced distribution of information with respect to the proposed inversion of the data, we carried out a subsampling of the original database, in several steps. First, for each period of swarm activity, we divided the swarm area into cubes with 1-km side length in each dimension. For each cube only the events with magnitudes larger than the mean magnitude were selected for the next step. Large number of events in a swarm usually occurs in a short period of time, therefore waveforms will overlap. Hence, in each cube, we furthermore selected only events with no overlapping waveforms. The number of events was reduced by these selection procedures from about 14 000 to about 2000 at this stage of the data preparation.

In order to avoid possible phase misinterpretations from automated routines all arrival times were manually re-picked using the SeismicHandler software of Stammler (1993). An example with analysed waveforms and corresponding traveltime picks is given in Fig. 3. Based on the arrival time weighting scheme of Evans *et al.* (1994) quality classes of 0 (highest), 1 and 2 were assigned to each traveltime pick regardless of wave type according to the estimated

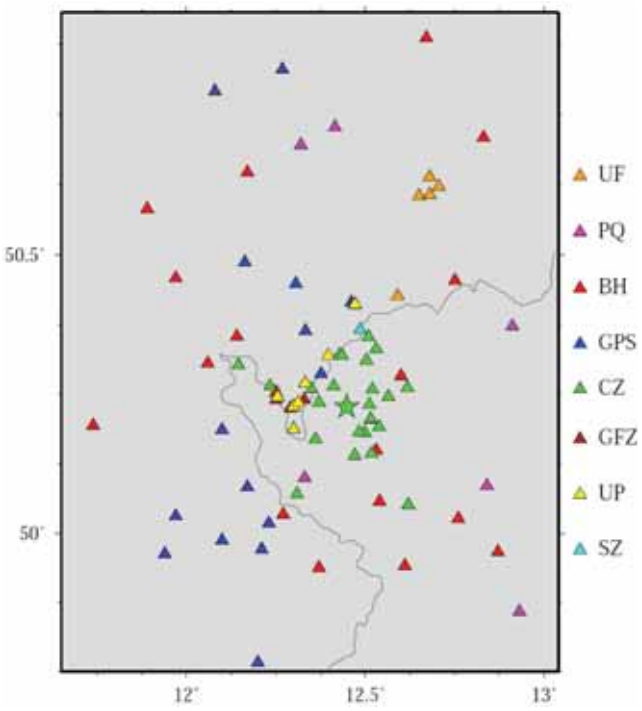

Figure 2. Distribution of seismological stations used in this investigation. The data were compiled by using stations from different sources: PASSEQ (PQ); BOHEMA (BH); German permanent stations (GPS); Czech Republic permanent stations (CZ); GeoForschungsZentrum Potsdam (GFZ); University of Potsdam (UP); University of Freiberg (UF); SZGRF (SZ). Reference station NKC shown with green star is used for delay time calculations.

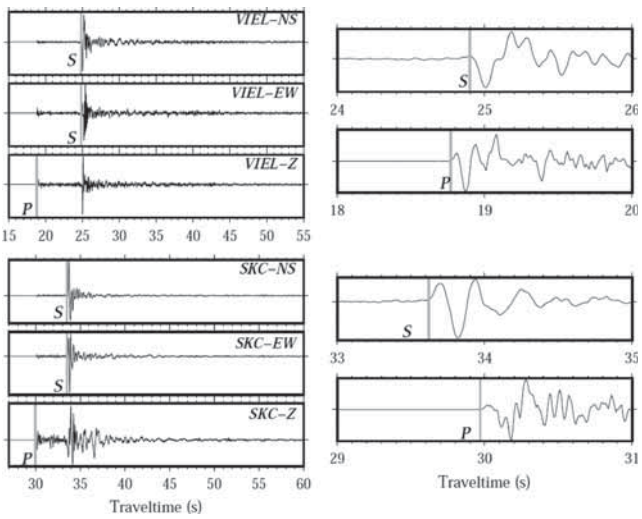

Figure 3. Data examples for an arbitrary chosen event (2008 October 12, 07:44:56.311 000 UTC, 12.447°E, 50.213°N, 9-km depth and magnitude of 3.8). Waveforms and traveltime picks of *P*- and *S*-wave arrivals are shown for one station from the WEBNET network (SKC) with 8-km epicentral distance and for another station from the BayernNetz network (VIEL) with 25-km epicentral distance.

picking accuracy of 0.025, 0.05 and 0.1 s, respectively. 88, 3 and 19 per cent of the *P* wave picks were in classes 0, 1 and 2. For *S* waves the corresponding numbers were 84, 6 and 10 per cent. The average picking error was 25.5 ms for *P* waves and 28.3 ms for *S* waves. For the subsequent 1-D and 3-D inversions, we only used events with a minimum number of six arrival times for *P* waves and

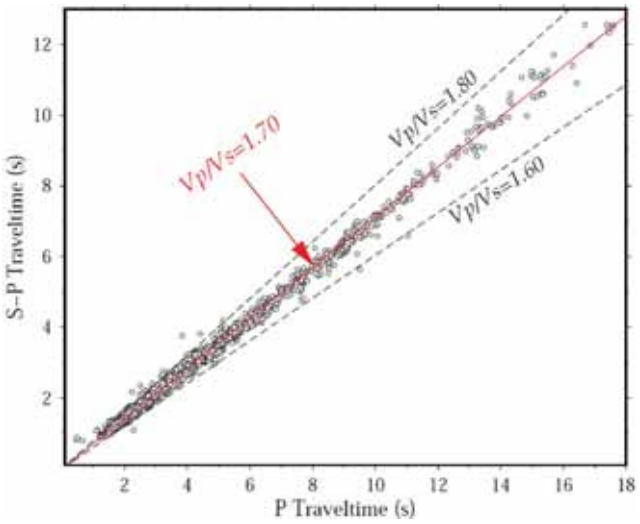

Figure 4. Wadati diagram derived from the traveltime data of 543 earthquakes. Linear regression provides an average Vp/Vs value of 1.70.

with a minimum number of six arrival times for *S* waves. Furthermore, an azimuthal gap criterion of 160° had to be fulfilled for each event. Magnitudes of the finally selected events vary between 0.5 and 4.5. Ultimately, the data set consists of 543 events with a total number of 13 378 picks including both *P* and *S* waves.

4 INVERSION OF TRAVELTIME DATA

4.1 1-D Reference model

Kissling *et al.* (1994) and Eberhart-Phillips (1986) proposed as a first step the simultaneous least-squares solution of the 1-D velocity model and hypocentre relocation which is called minimum 1-D model. The intention of defining a 1-D velocity model is that it is used for earthquakes relocation and also as an initial model for the 3-D inversion. Defining the minimum 1-D velocity model is a trial and error procedure (Kissling *et al.* 1994), as the solution may strongly depend on the starting model. To consider all possible solutions, we have started with a wide range of initial velocity–depth functions including both realistic and unrealistic models as suggested by Boncio *et al.* (2004). This approach ensures that all possible solutions have been considered. The ratio of Vp/Vs was initially defined as 1.70 based on the analysis of the Wadati diagram (Fig. 4). This value is in agreement with the average Vp/Vs of 1.7 for West Bohemia as determined by Málek *et al.* (2005). Station NKC (green star in Fig. 2) was chosen as the reference station based on its central location in West Bohemia and because of a high number of event recordings. We used the VELEST (Kissling *et al.* 1995) program and started with 100 random *P*-wave velocity models. The models consist of layers with 1-km thickness. Other layer thickness values were tested as well. From these tests we conclude that the choice of the layer thickness was not a critical parameter as similar inversion results were generated for different layering models. A random velocity value between 4 and 7.5 km s^{-1} was assigned to each layer. After completion of the inversion process, all models converged to similar velocity–depth functions in the depth range between 3 and 12 km where hypocentres were located and that contain the highest density of ray coverage. The final minimum 1-D velocity model is the model with minimum RMS residuals among all output models and is indicated by a red line in Fig. 5. All models (grey lines) show a strong increase of Vp with increasing depth within the upper layers of the model and reaching values of around 6 km s^{-1} below 5 km depth. The 1-D inverse modelling using VELEST also included the inversion for Vs and relocation of hypocentres. The RMS error for the chosen minimum 1-D model was around 60 ms. Compared to the average picking error of our data, the relatively high value of final RMS of 60 ms was due to 3-D structure that could not be modelled by a minimum 1-D model. To estimate the 'absolute error' (Kissling 1988) in location of the hypocentres, we relocated 30 shots which had 12 or more *P*-wave arrivals (see Růžek & Horálek (2013) and references therein) using

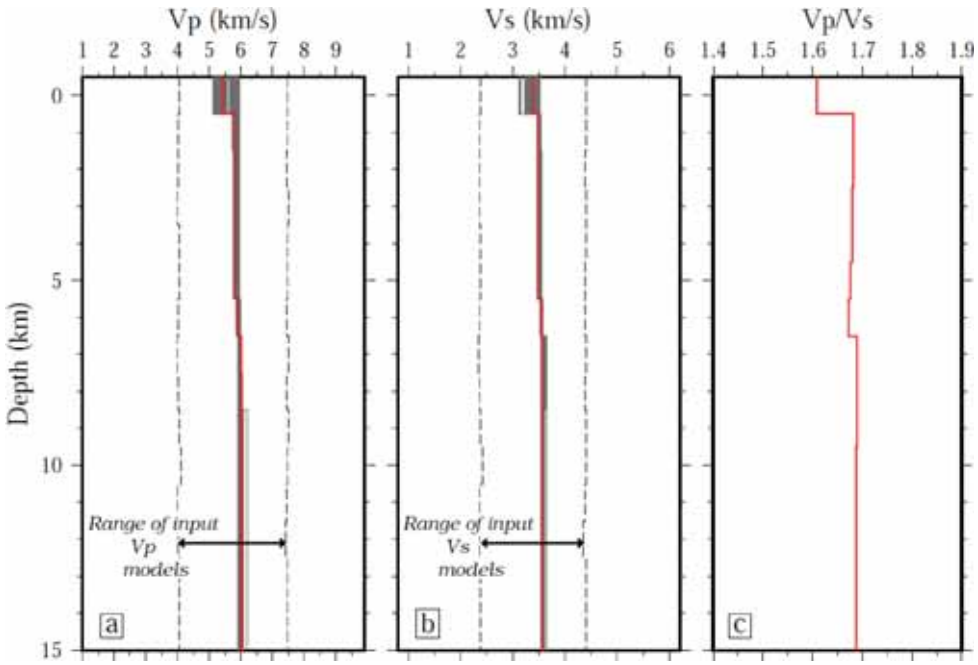

Figure 5. Final minimum 1-D velocity model for (a) *P*-wave, (b) *S*-wave and (c) Vp/Vs ratio. All output models are indicated by the grey lines. Solid red lines indicate the best final model with lowest RMS. The range of input models are indicated by the thin dashed black lines.

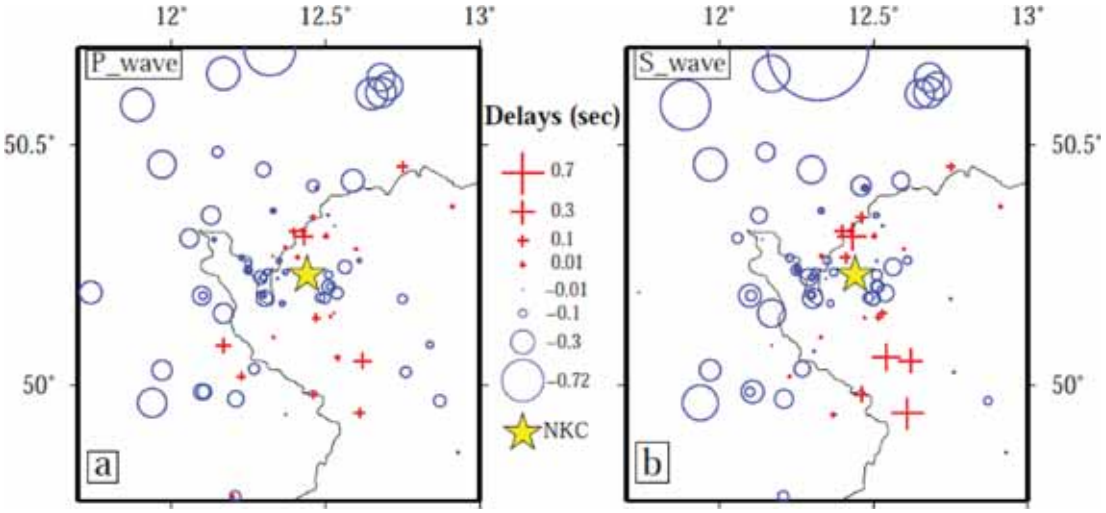

Figure 6. Station delay times determined for *P*- and *S*-wave arrivals based on the results of the 1-D inversion. Red crosses and blue circles indicate the polarity and size of station delay times relative to the reference station (NKC) which is marked as a yellow star.

our final 1-D velocity model. The maximum mislocation of shots in latitude, longitude and depth is less 1 km, however for majority of them it is less than 0.5 km. It is obvious that the mislocation error for shots is higher than that of earthquakes since the corresponding ray paths for earthquakes are less affected by near-surface heterogeneity (Kissling 1988).

4.2 Station corrections

Station corrections represent lateral variations of data fitting within the 1-D velocity model (Kissling *et al.* 1995). Variations in station corrections can reflect near-surface heterogeneity (for stations within a network) and large-scale velocity variations (for peripheral stations). The magnitude of station corrections reflects the local geology of the study area. Positive values of station corrections indicate that velocities are slower and negative values indicate that velocities are higher beneath the station compared to the 1-D velocity model. Fig. 6 shows the calculated station corrections for *P* and *S* waves. Station delay times relative to the reference station NKC are observed in the range of −1.3 to +0.7 s. The anomalies are most likely related with local features such as the Cheb basin, which deviate from the average velocity structure estimated by the 1-D inversion.

4.3 3-D Tomographic model

After estimating a proper reference 1-D velocity model we applied the traveltime tomography program SIMUL2000 (Thurber 1983, 1993; Eberhart-Phillips 1993). The package allows for the simultaneous inversion for hypocentre locations and 3-D isotropic velocity structure (Vp and Vp/Vs). Forward calculations to predict traveltimes and ray paths are carried out using a pseudo-bending method (Um & Thurber 1987). A damped least-squares algorithm is applied to determine model parameter updates for velocities and hypocentre locations during the iterative inversion. Noteworthy, the inversion is carried out for Vp and Vp/Vs instead of Vp and Vs to address the generally lower resolution of the Vs model, which is typically related with problems to determine *S*-wave arrival times with high accuracy (Thurber 1993; Thurber & Eberhart-Phillips 1999).

The starting models for the tomographic inversion was constructed following the recommendations given by Evans *et al.* (1994). The initial *P*-wave velocity model and initial earthquake locations were based on the optimum 1-D model inversion using VELEST. For the initial Vp/Vs model we used a uniform value instead of a 1-D Vs starting model. A constant Vp/Vs of 1.70 was applied based on the Wadati diagram analysis (Fig. 4). During the next steps, the grid node spacing was continuously decreased during the iterative inversion work flow as suggested by Evans *et al.* (1994). The horizontal node spacings were successively reduced, starting at 20 km spacings and finishing with 4 km spacings during the final inversion. Vertical nodes were spaced with 3 km during the entire inversion work flow. To address for the heterogeneous ray coverage, node spacings were enlarged in the outer parts of the model (Fig. 7).

Adequate damping parameter values were determined based on test inversions where a wide range of potential damping parameter values were applied. Trade-off curves generated from these tests are shown in Fig. 8. Optimum damping values of 100 for the Vp inversion and 200 for Vp/Vs inversion were chosen to balance between a sufficient data misfit reduction and a weak model variance. Although trade-off curve for Vp/Vs suggests smaller optimum damping value (around 100), we chose 200 to obtain smoother results.

4.4 Resolution tests

The presentation and discussion of the final inversion results requires knowledge of resolution of the derived tomographic models. A first impression of resolution can be obtained by plots of the ray paths used in the tomographic inversion (Fig. 7). High resolution can be expected when a large number of rays are travelling in different directions within a given subvolume of the model. To better quantify the resolution for each grid node, we have analysed the full resolution matrix provided within the SIMUL2000 package.

Here we make use of spread function (SF) which was calculated from the full resolution matrix based on the procedure described in Eberhart-Phillips & Michael (1998). The SF considers both diagonal elements and off-diagonal elements of the resolution matrix and, hence, it is reflecting the sensitivity of model nodes as well as the degree of smearing of information over neighbouring model regions. The advantage of the SF is that the information described

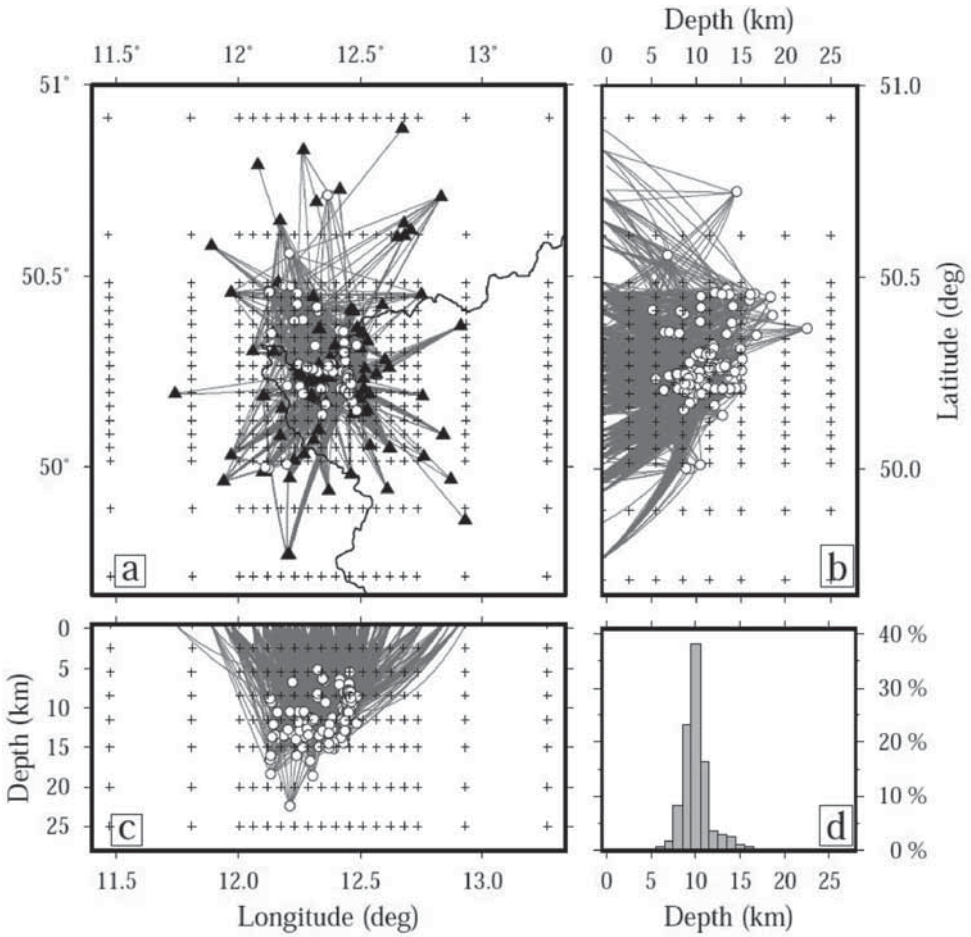

Figure 7. Map view and vertical sections show ray paths between earthquakes (white circle) and receiver stations (black triangles) for selected seismic events. The model grid nodes are indicated by black crosses. Histogram plot shows the depth distribution of earthquakes.

within one row of the resolution matrix is compressed into a single number which can be displayed easier than the full matrix information (Toomey & Foulger 1989). Results are shown in Fig. 9. Generally, low SF values are indicating high resolution and *vice versa*. The pattern of resolution is similar for Vp and Vp/Vs. The highest resolution is reached in the central part of the model where the swarm cluster is located.

Another possibility to evaluate the resolving power of the tomography is to generate synthetic data from theoretical models and try to reconstruct the given model by using the inversion algorithm. For such a test inversion we defined a model with blocks of 10 per cent positive and negative anomalies for Vp and Vp/Vs (Fig. 10) which mimics the characteristic features of the real data inversion results as can be seen in the next section. The geometry of the anomalies was defined independently in Vp and Vp/Vs because we cannot assume that both parameters are correlated in each case. Actually, using such a pattern of independent Vp and Vp/Vs anomalies is even a more challenging task for the inversion algorithm than a coupled anomaly pattern. The source and receiver locations were chosen identical to the real experiment. Synthetic traveltimes were calculated within SIMUL2000, and Gaussian noise in accordance with the pick uncertainty weighting scheme was added to simulate similar conditions as observed for the real data. The results of the tomographic reconstruction of the synthetic test models are shown in Fig. 10. Red and blue boxes show the outline of synthetic low and high velocity anomalies. The features mostly could be recovered by the inversion. As expected, the anomalies are getting more smeared in the deeper parts and outer regions of the model. A comparison with Fig. 9 confirms that the well-resolved parts of the characteristic model show SF values smaller than 2.5, and that such a value can be used to identify well-resolved parts in the results as presented below. It should be mentioned that we kept the hypocentres fixed during the inversion process for the synthetic test. This may produce a slight bias towards a favourable recovery of the original model, but given the high accuracy of original hypocentre locations in the real dataset, this will not be of significant importance.

5 RESULTS

The results of the 3-D tomographic inversion for Vp and Vp/Vs are presented in Figs 11–13. The RMS error for the final model was about 35 ms, slightly above average picking error. We show four horizontal slices and four vertical sections to visualize the major features of the model. The images were interpolated from the inversion grid by applying the identical interpolation method as used in forward and inverse calculations within SIMUL2000. Horizontal slices of Vp (Fig. 11) and Vp/Vs (Fig. 12) are plotted at the vertical nodes of the final inversion grid, at 2.5, 5.5, 8.5 and 11.5 km depth. Note that we shifted the depth of grid nodes, sources and receivers

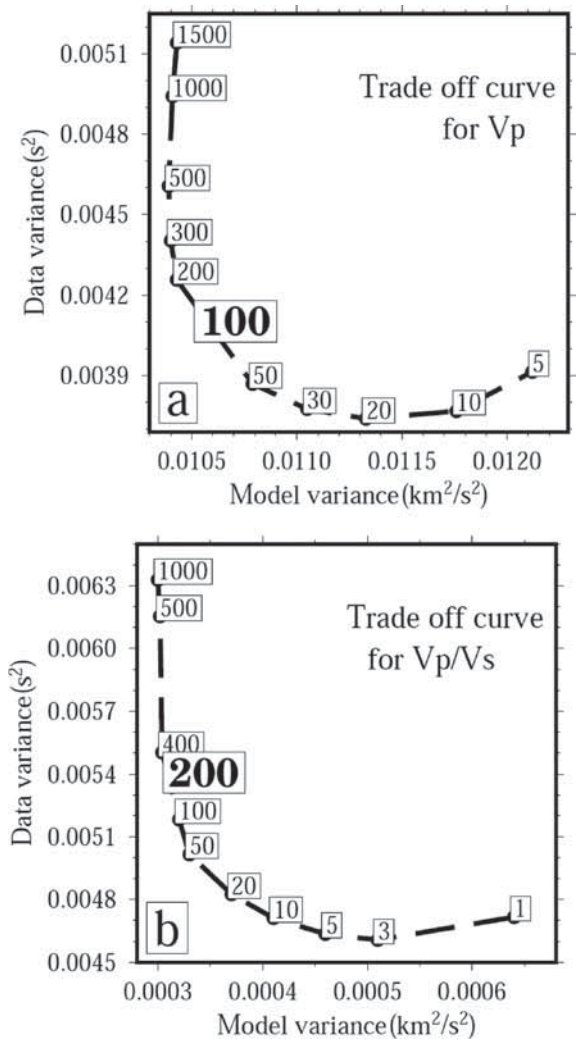

Figure 8. Trade-off curves used for the determination of optimum damping parameter values used in the damped least-squares inversion. A value of 100 was chosen for Vp and 200 for Vp/Vs.

by 500 m and inverted at 0, 3, 6, 9 and 12 km. Later for the presentation of results, we were undoing the depth shift. These map views also include the surface projection of the seismicity as well as the outline of the Cheb basin and the location of the Bublák/Hartoušov mofette fields. The vertical sections along profiles A–D (Fig. 13) are crossing major structures such as the earthquake swarm region and the Cheb basin. A lateral, perpendicular projection of seismic events is displayed in these vertical sections, if the projection distance is smaller than 1 km (Fig. 13). For orientation, the location of the profiles A–D can be found within the horizontal slices of Vp (Fig. 11) and Vp/Vs (Fig. 12).

The most prominent feature resolved within the upper crust is an anomaly of relatively low-Vp values, which coincides with the outline of the Cheb basin. Within this body the *P*-wave velocities vary between 4.7 km s^{-1} at the surface and 5.5 km s^{-1} at 2.5 km depth (Fig. 13, profile B). Another, slightly smaller feature with similar lower *P*-wave velocities is located north of the Cheb basin in the border region between Germany and Czech Republic. At the location of these low-Vp anomalies, we observe increased Vp/Vs ratios, which, however, are slightly smaller in size compared to the low-Vp anomalies (Fig. 13). The high-Vp/Vs spot within the Cheb basin corresponds to the location of the Bublák/Hartoušov mofette fields.

Another pronounced upper crustal anomaly was imaged at the western edge of the resolved area. This feature is represented by a circular anomaly of high Vp/Vs around the western end of profile B at 2.5 km depth (Fig. 12). A corresponding high-Vp anomaly is found but this is not coinciding perfectly with the circular Vp/Vs feature and it is slightly shifted northward. Based on the resolution tests using the characteristic model recovery approach we have to assume that a larger degree of smearing is degrading the reliability of this structure. Hence, this feature was not considered in our interpretations.

In the deeper parts of the model, at mid-crustal level, the most prominent feature is imaged just below the swarm hypocentres. Within the horizontal slice at 11.5 km depth the anomalous regions shows high-Vp values of 6.5 km s^{-1} (Fig. 11) and increased Vp/Vs values of 1.75 in comparison with the average value of 1.7 (Fig. 12). The structure is covering parts of the swarm cluster region around Nový Kostel and extends further northward as far as the Czech–German border. At 11.5 km depth it has a diameter of about 9 km. The anomalous body of high Vp and increased Vp/Vs is changing its shape to a more complex and heterogeneous feature at shallower depth where it can be followed up to the 8.5 km depth slice in Vp (Fig. 11) and in Vp/Vs (Fig. 12).

6 DISCUSSION

Combining Vp and Vp/Vs in the interpretation of tomographic models is an efficient approach to better constrain the lithological nature of the subsurface in comparison with the separate consideration of each parameter (e.g. Bauer *et al.* 2003). Vp is particularly suited to distinguish between sediments showing low-Vp values and the hard rock basement which is characterized by Vp values larger than 5.5 km s^{-1}. Moreover, very high crustal velocities are typically associated with igneous rocks whereby larger portions of mafic components may further increase Vp. The ratio of Vp/Vs can provide additional constraints on the mineral composition (Christensen 1996). To give some examples, quartz as an important rock-forming mineral has a very low Vp/Vs and, hence, granites and felsic material in general are characterized by decreased Vp/Vs whereas mafic rocks show Vp/Vs higher than average values (Christensen 1996). Furthermore, Vp/Vs is rather sensitive to the presence of fluids where a high fluid content is often related with increased Vp/Vs values. The relation between Vp/Vs and fluid content is, however, complicated by additional influences of pore space geometry and pore pressure (e.g. Nur & Simmons 1969; Mavko & Mukerji 1995; Takei 2002). In the following, we interpret the lithological nature of the major features in our Vp and Vp/Vs tomograms and discuss their possible relation to the earthquake swarm around Nový Kostel.

6.1 Cheb basin shows low-Vp anomaly

Our tomography study reveals for the first time a velocity anomaly, which reflects the geometry of the Cheb basin (see dashed outline in Figs 11 and 12). The tomographic investigations of Růžek & Horálek (2013) and Alexandrakis *et al.* (2014) did not provide hints for such an anomaly. The larger number of seismological stations used in our case might be the reason for this difference. Low-to-moderate Vp values between 4.7 km s^{-1} at the surface and 5.5 km s^{-1} at 2.5 km depth indicate that the basin is not filled

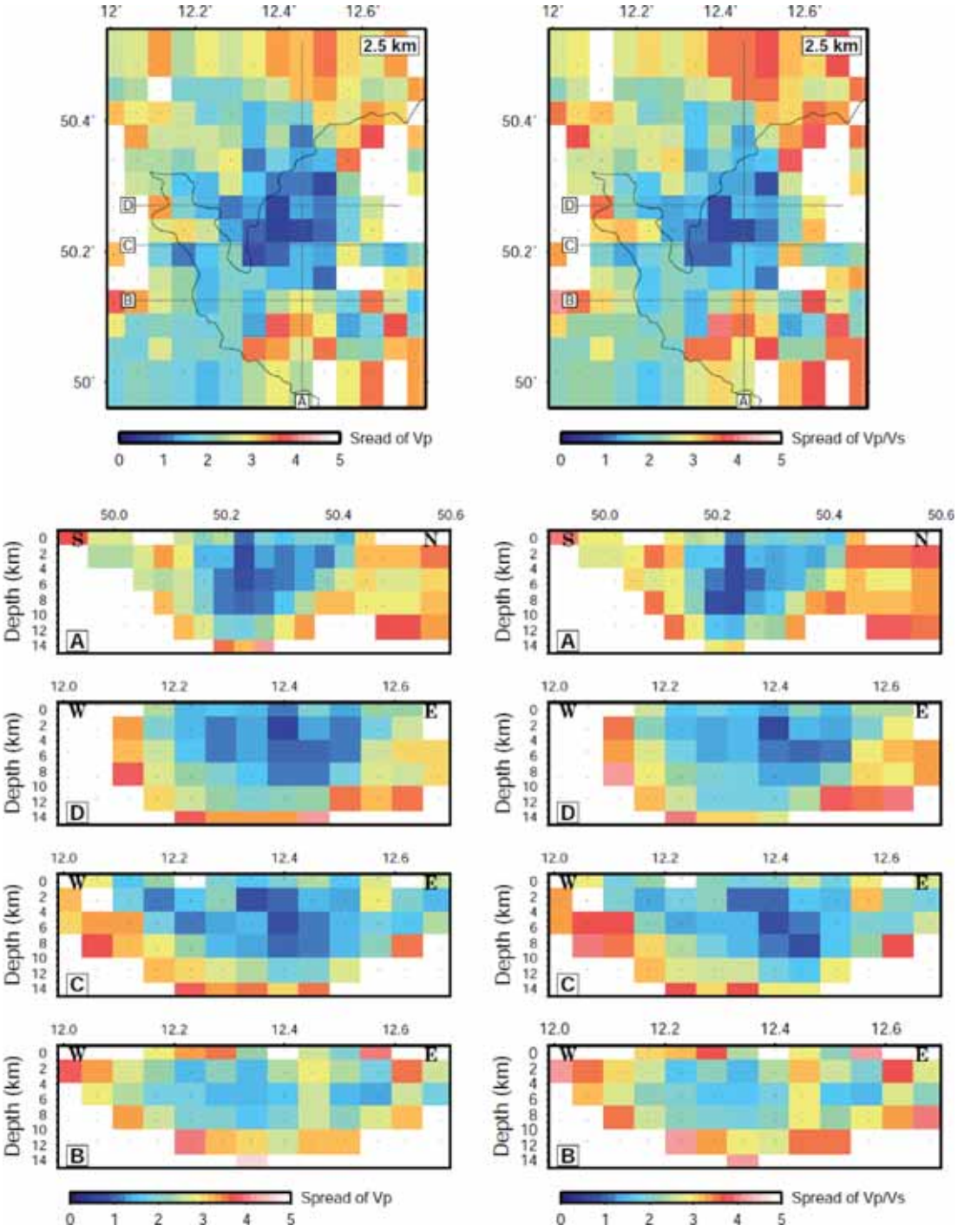

Figure 9. Map views and vertical sections showing SF values to illustrate the resolution of the tomographic models for Vp and Vp/Vs. SF values were calculated from the full resolution matrix. The location of the vertical sections is indicated within the map views.

by very soft and unconsolidated material (Figs 11 and 13). This could be related with a predominant input of eroded crystalline hard rocks from the surrounding Bohemian Massif into the basin. Remarkably, we see no continuation of the Cheb basin velocity anomaly into the Eger rift. From this observation we infer a particular role of the Cheb basin within the rift system. Deeper rooted updoming, extensional or more complex processes, or possible effects from very localized crustal and sub-crustal structures can be assumed to explain the local character of the basin. Noteworthy, north of the Cheb basin we observe a slightly smaller and shallower basin structure with similar *P*-wave velocities as imaged within the 2.5-km depth slice (Fig. 11). To our knowledge, this was not named as a distinct geological feature so far.

Underneath and outside of the Cheb basin and the smaller basin to the North, *P*-wave velocities show values in the range of 5.7–5.9 km s^{-1} near the surface and values of 6–6.2 km s^{-1} at upper crustal levels. These observations are in agreement with an interpretation of a predominantly granitic composition for the abundant

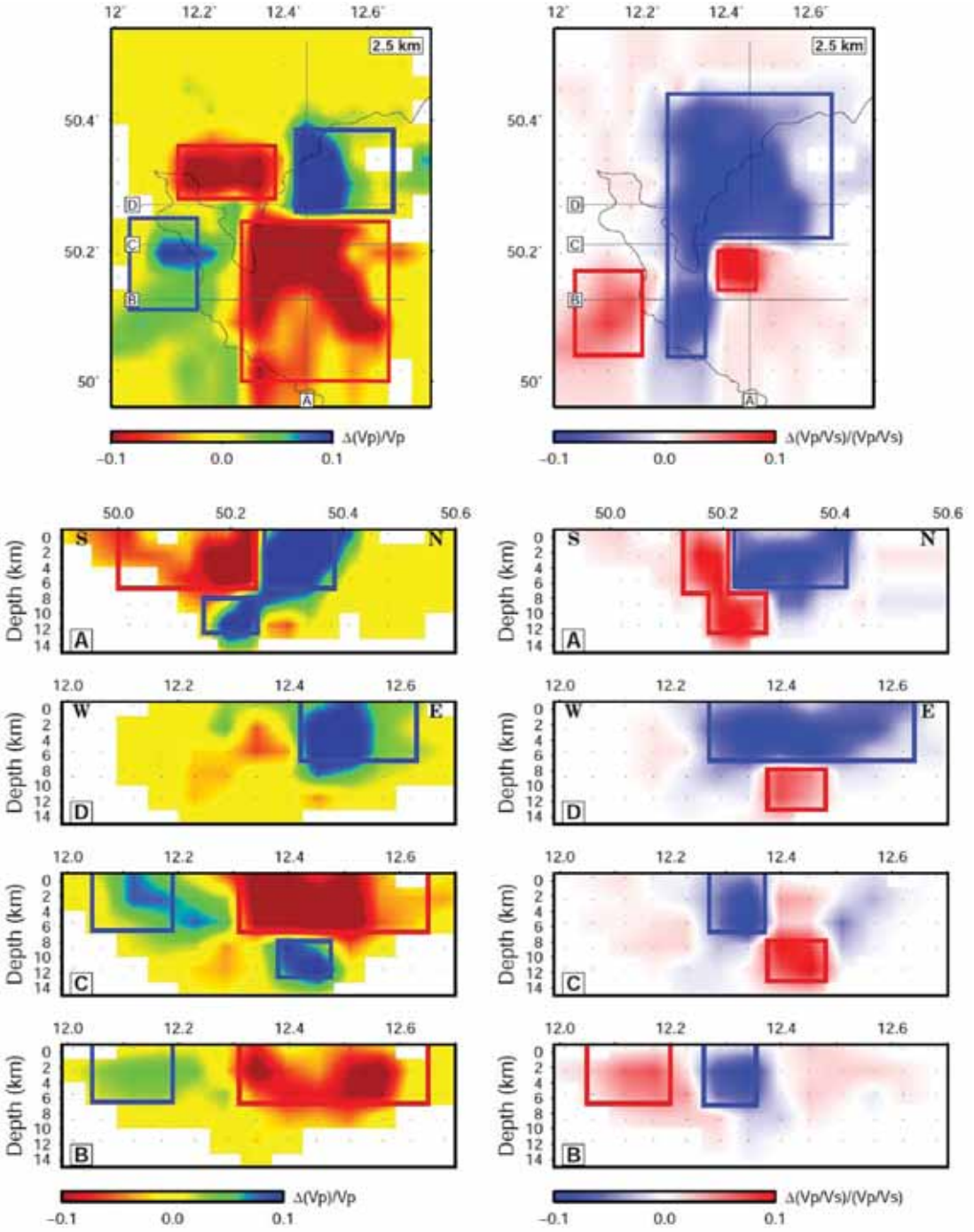

Figure 10. Recovery of theoretical models derived from the inversion of synthetic data. A pattern of characteristic anomalies was defined to generate the theoretical model. Blue and red boxes indicate the geometry of negative and positive anomalies. The anomalies were defined independently in Vp and Vp/Vs.

crystalline rocks of the Bohemian Massif. This interpretation is also supported by the estimation of *in situ* Vp values for granitic rocks within the study area based on laboratory measurements (Pros *et al.* 1998). The distribution of Vp/Vs values is not showing a simple pattern which could be used to distinguish between basin sediments and the crystalline basement. At least, there is a tendency of higher Vp/Vs values found within the central parts of the basin regions (Fig. 12). This can be explained by generally larger porosity in sedimentary rocks and the related capacity to absorb larger amounts of fluids.

6.2 Fluid outflow at the Bublák/Hartoušov mofette fields

As an interesting observation we found a steep channel of high Vp/Vs within the Cheb basin (Fig. 12 and profile A in Fig. 13). It can be followed from the surface down to about 4 km depth. If only the geometry is considered, the channel can be further tracked down to the location of the earthquake swarm (profile A in Fig. 13). Along this way, Vp/Vs is changing from increased values of 1.75 at the surface to average values of 1.7 within the swarm cluster. The surface outcrop of the anomaly coincides with the location of the Bublák/Hartoušov mofette fields.

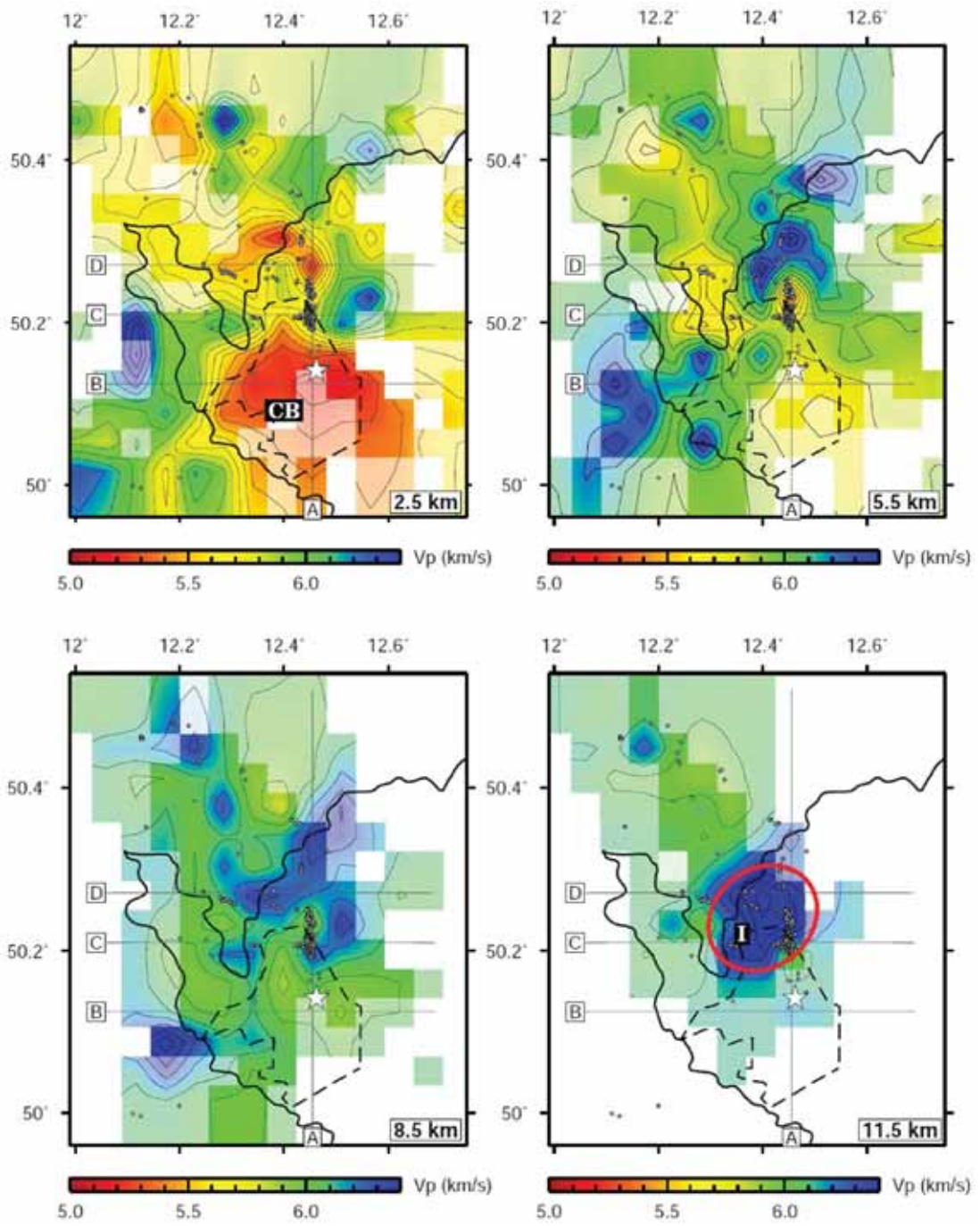

Figure 11. Horizontal slices show the final Vp distribution at 2.5, 5.5, 8.5 and 11.5 km depths. Regions with less resolution are shown faded, and non-resolved parts are blank. The location of profiles A, B, C and D are given for orientation. Seismic event locations are plotted as grey circles. The outline of the Cheb basin (CB) is shown as a dashed line. A mid-crustal intrusive anomalous body (I) is outlined by a red ellipse at 11.5 km depth. The white star indicates the location of the Bublák/Hartoušov mofette fields.

Our interpretation is that the channel represents a pathway for fluids which originate from magmatic sources in the deeper crust or upper mantle which are passing the earthquake swarm focal zone. The fluids reduce the shear strength and stimulate earthquakes within the swarm focal zone. This argumentation is following the proposed scenario suggested by Weise *et al.* (2001) which was based on geochemical sampling of fluids and gas emissions measured at the Bublák mofette. The Vp/Vs within this channel is highest in the upper, sedimentary parts of the fluid pathway because of the potentially high porosity in sedimentary rock. Within the deeper parts of the pathway, down to the depth of the earthquake swarms, the Vp/Vs values are still larger than in the surrounding upper crustal rocks. We assume that fluids are transported along fractures in this part of the channel.

6.3 Seismic properties within swarm focal zone

Vp/Vs values found within the swarm focal zone are in agreement with a previous study by Dahm & Fischer (2013). However,

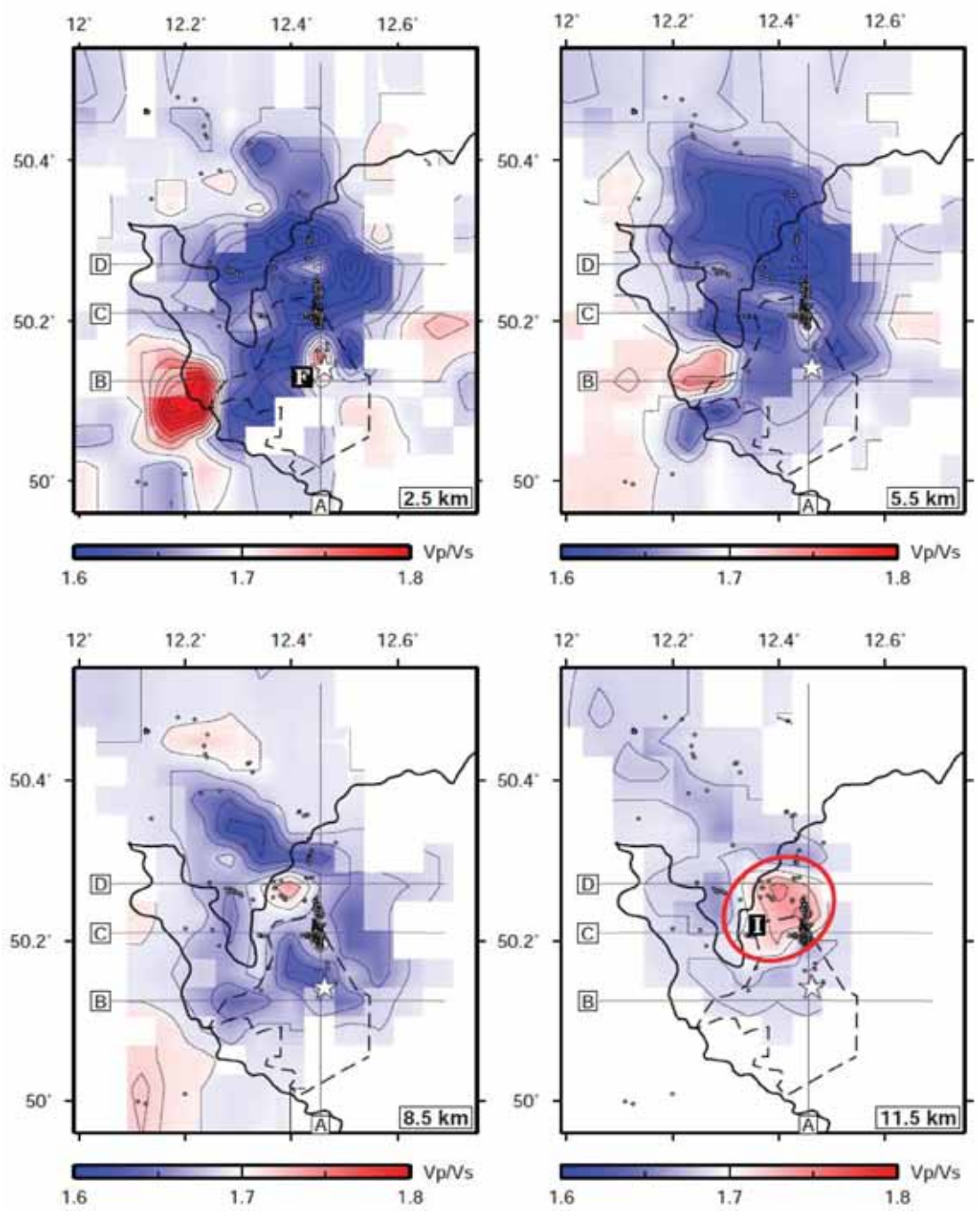

Figure 12. Horizontal slices show the final Vp/Vs distribution at 2.5, 5.5, 8.5 and 11.5 km depths. Regions with less resolution are shown faded, and not-resolved parts are blank. The location of profiles A, B, C and D are given for orientation. Seismic event locations are plotted as grey circles. The outline of the Cheb basin is shown as a dashed line. Labelled features F (fluid pathway) and I (mid-crustal intrusive body) are discussed in the text. The white star indicates the location of the Bublák/Hartoušov mofette fields.

a detailed comparison should be considered carefully, because we derived our tomographic models based on a longer period of seismicity observations whereas Dahm & Fischer (2013) focussed on temporal changes of Vp/Vs before, during and after single swarms. Dahm & Fischer (2013) used double-differences in traveltimes for pairs of earthquakes to estimate Vp/Vs values within the swarm region. Inside the focal zone they found short periods of strong decrease in Vp/Vs as low as 1.33 during the initiation of swarm activities and an increase to saturation values of around 1.7 when the swarm decays. According to Dahm & Fischer (2013) the very low-Vp/Vs values could be explained by overpressurized gas in the establishing phase of the swarm. Our tomography delivered velocity ratios of around 1.7 in the earthquake swarm region similar to the values determined by Dahm & Fischer (2013) when only the background seismicity was considered. Values of around 1.7 are not very high compared to global average Vp/Vs values. However, these values in the focal zone are still larger than within the surrounding granitic crust where values of around 1.65 are obtained

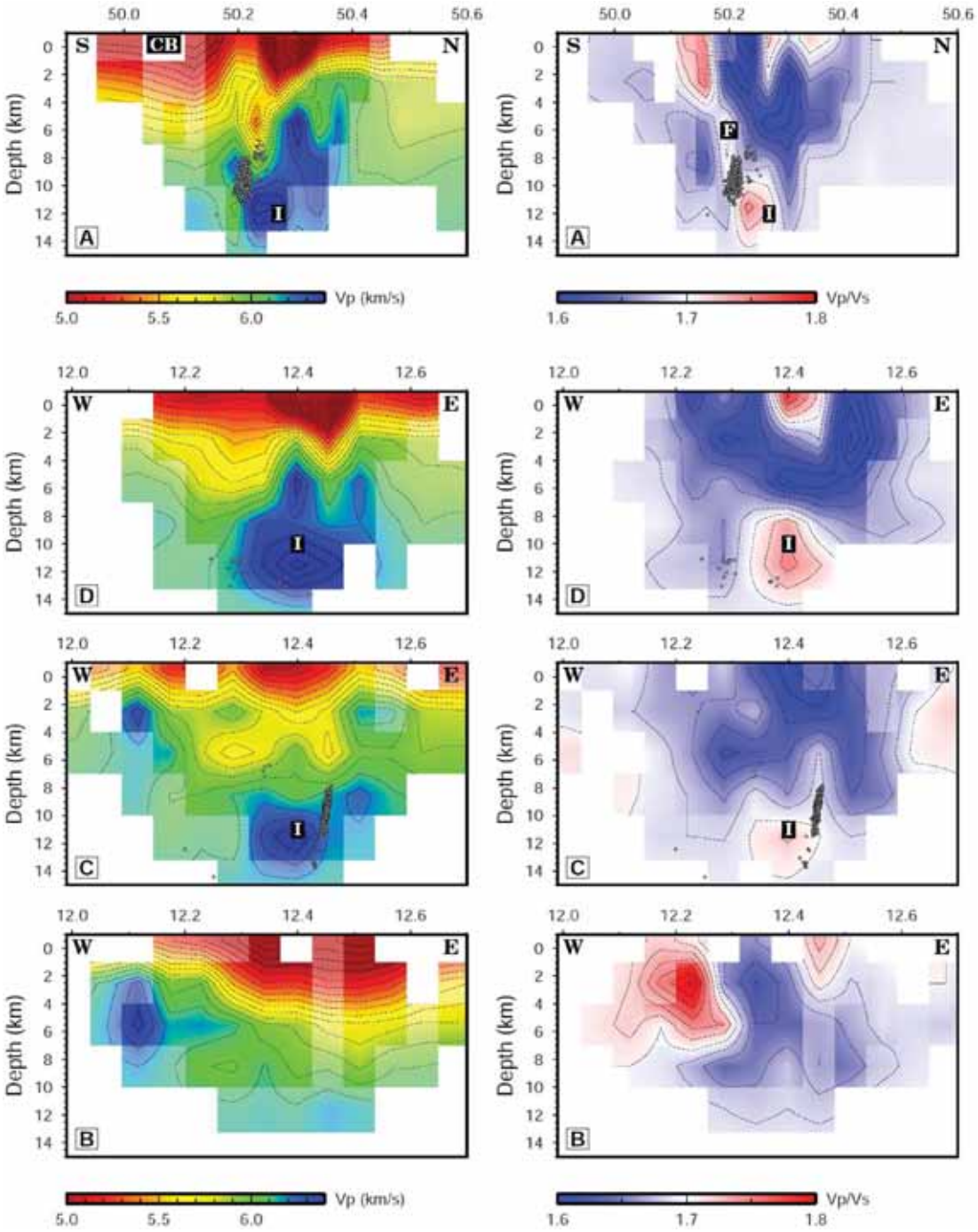

Figure 13. Vertical sections showing the final Vp and Vp/Vs distributions along profiles A, B, C and D. The location of the profiles is given in Figs 11 and 12. Regions with less resolution are shown faded, and not-resolved parts are blank. Seismic events are plotted if the horizontal projection distance is smaller than 1 km. Labelled features CB (Cheb basin), F (fluid pathway) and I (mid-crustal intrusive body) are described in text.

(Fig. 13). In our interpretation the slightly increased Vp/Vs values are related to fluids which are passing the fractured earthquake zone.

Considering Vp, the swarm focal zone cannot be associated with a distinct anomaly. Tentatively, we would expect low *P*-wave velocities as an effect of fracturing and damaging within such a zone of repeating seismicity. Instead, the earthquakes are located in a transition zone between normal crust and a high velocity crustal body imaged below and north of the swarm (Fig. 13).

6.4 Mid-crustal intrusive body stimulates fluid flow and earthquake swarms

Our tomography revealed an anomalous crustal body located just below and north of the earthquake swarm zone. The feature is most obvious at the 11.5 km depth slices of Vp (Fig. 11) and Vp/Vs (Fig. 12) where it is highlighted by a red-coloured ellipse. *P*-wave velocities reach values as large as 6.5 km s^{-1} within the anomaly against average values of about 6 km s^{-1} in the surrounding crust (Fig. 11). A similar pattern is imaged by Vp/Vs (Fig. 12). With

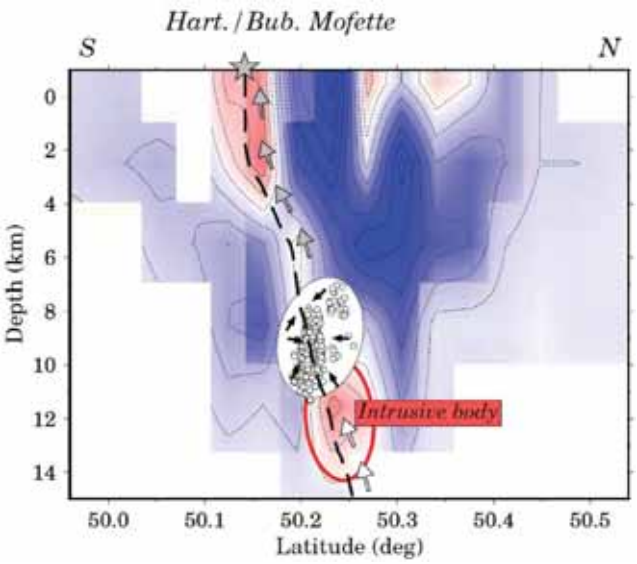

Figure 14. Conceptual model showing major crustal features as imaged and interpreted in this study. The coloured background represents the Vp/Vs distribution along profile A (Fig. 13). The indicated intrusive body was first identified and interpreted within the 11 km depth slices of Vp (Fig. 11) and Vp/Vs (Fig. 12). Potential fluid pathways are identified based on a channel-like increased Vp/Vs structure. Crustal fluids and supercritical fluids from greater depths may trigger earthquakes and are mixed before their ascend to the Bublák/Hartoušov mofette fields.

reference to the average value of 1.70 derived by the Wadati diagram (Fig. 4), we observe increased velocity ratios within the zone of high Vp and decreased velocity ratios in the surrounding crust. Assuming a lithostatic pressure of larger than 300 MPa at 11 km depth and referring to petrophysical data presented by Christensen (1996) the anomaly values of 6.5 km s^{-1} in Vp and 1.75 in Vp/Vs can be assigned to a Diorite composition. The surrounding crust with Vp values of around 6 km s^{-1} and Vp/Vs values of around 1.65 can be explained by a quartz-rich granitic composition. Considering the distribution and juvenescent shape of the anomalous body at shallower depths (Fig. 11) we interpret the anomaly as a solidified igneous body which intruded into a reactivated crust during the formation of the Cheb basin and Eger rift. Alternatively, the intrusive body could be older than the basin and rift structures, and, possibly, influenced the location of the extensional features.

Many tomographic studies show pronounced velocity and Vp/Vs ratio anomalies in earthquake swarm areas (e.g. Husen *et al.* 2004; Vidale & Shearer 2006; Lin & Shearer 2009; Kato *et al.* 2010; Muksin *et al.* 2013). These studies implied that non-volcanic seismic swarms are related to fluid movements. For West Bohemia, Weise *et al.* (2001) supposed that earthquake swarms are triggered by supercritical fluids ascending from deeper magmatic sources occurring within the mantle or around Moho depths. The earthquake processes could lead to a mixing of deep-sourced supercritical fluids and crustal fluids, which further propagate to the surface along potential fluid pathways (Weise *et al.* 2001). Our tomography brings a new feature into this proposed scenario. As shown in Fig. 14, we assume that the found intrusive body could be part of the fluid pathway from the mantle through the earthquake zone up to the Bublák/Hartoušov mofette fields at the surface. Additionally, we speculate that enhanced fluid flow could be driven by a thermal anomaly associated with the assumed solidified intrusion if cooling is not fully completed. Kato *et al.* (2010) imaged high-Vp and high-Vp/Vs anomalies below a cluster of earthquakes on a non-volcanic earthquake swarm system in Japan. Similar to our study, the anomaly was interpreted as a solidified intrusive body which contributes to the triggering of earthquakes by feeding fluids into the swarm focal zone. The intrusive body represents a pronounced heterogeneity within the crust and this might lead to increased stress which could contribute to the triggering of earthquakes in the swarm focal zone. Subsequently, stress changes in the vicinity of intrusive bodies are assumed to control the position of swarm activity (e.g. Dahm *et al.* 2008).

7 CONCLUSIONS

We presented results from a new LET study for the earthquake swarm region in West Bohemia (Czech Republic)/Vogtland (Germany). Using a large number of widely distributed seismological stations, more details of Vp and Vp/Vs in the upper and middle crust could be revealed in comparison with previous investigations.

For the first time, the Cheb basin and the Bublák/Hartoušov mofette fields located within the basin are imaged by distinct Vp and Vp/Vs anomalies and a high-Vp/Vs channel could be tracked down to the earthquake swarm hypocentres. We proposed that this is the image of a fluid pathway. A new feature with high Vp and increased Vp/Vs was found below and north of the swarm focal zone. We interpreted this anomaly as a solidified intrusive body which emplaced prior or during the formation of the Eger rift and Cheb basin. Earthquakes are concentrated at the southern boundary of the assumed intrusive body, at the junction of the rift and the basin. We assumed that the solidified intrusive body is providing fluids and gas which propagate towards the earthquake swarm focal zone along pathways formed along weak structures at the junction of the rift system and the MLF zone. The intruded mid-crustal body might contribute to the triggering of the earthquakes not only by delivering fluids into the focal zone. We speculate that the intrusive body also leads to stress accumulations particularly at the junction of the Eger rift, Cheb basin and MLF. This could potentially support the triggering of earthquakes in the swarm focal zone.

Future work should focus on the confirmation of the imaged structures by using different geophysical methods. Our interpretation could be furthermore tested from the perspective of geochemical sampling of fluids at the surface which potentially allows independent inferences on the composition of the source rocks and pressure and temperature conditions at depth.

ACKNOWLEDGEMENTS

We thank a number of colleagues for valuable support during different stages of this study. Data were provided by GFU in Prague, with support of Josef Horálek and Bohuslav Růžek. We are thankful for contribution of Dirk Roessler in early stages of this project. Siegfried Wendt from Collm observatory provided advice in picking of events. We wish to thank Christian Haberland and Umar Muksin for support in the usage of SIMUL2000 and related software. SM was funded by Deutsche Forschungsgemeinschaft (DFG) within the framework of SPP-1006. We would like to thank two anonymous referees for their useful comments and suggestions for the manuscript.

REFERENCES

Alexandrakis, C., Caló, M., Bouchaala, F. & Vavryčuk, V., 2014. Velocity structure and the role of fluids in the West Bohemia Seismic Zone, *Solid Earth,* **5,** 863–872.

Babuška, V., Plomerová, J. & Vecsey, L., 2008. Mantle fabric of western Bohemian Massif (central Europe) constrained by 3D seismic P and S anisotropy, *Tectonophysics,* **462,** 149–163.

Bankwitz, P., Schneider, G., Kämpf, H. & Bankwitz, E., 2003. Structural characteristics of epicentral areas in Central Europe: study case Cheb basin (Czech Republic), *J. Geodyn.,* **35,** 5–32.

Bauer, K., Schulze, A., Ryberg, T., Sobolev, S.V. & Weber, M.H., 2003. Classification of lithology from seismic tomography: a case study from the Messum igneous complex, Namibia, *J. geophys. Res.,* **108**(B3), 2152, doi:10.1029/2001JB001073.

Boncio, P., Lavecchia, G., Milana, G. & Barbara Rozzi, B., 2004. Seismogenesis in Central Apennines, Italy: an integrated analysis of minor earthquake sequences and structural data in the Amatrice Campotosto area, *Ann. Geophys.,* **47,** 1723–1726.

Bräuer, K., Kämpf, H., Strauch, G. & Weise, S.M., 2003. Isotopic evidence (^{3}He/^{4}He, $^{13}C_{CO2}$) of fluid-triggered intraplate seismicity, *J. geophys. Res.,* **108**(B2), 2070, doi:10.1029/2002JB002077.

Bräuer, K., Kämpf, H., Niedermann, S. & Strauch, G., 2005. Evidence for ascending upper mantle-derived melt beneath the Cheb basin, central Europe, *Geophys. Res. Lett.,* **32,** L08303, doi:10.1029/2004GL022205.

Bräuer, K., Kämpf, H. & Strauch, G., 2009. Earthquake swarms in non-volcanic regions: what fluids have to say, *Geophys. Res. Lett.,* **36,** L17309, doi:10.1029/2009GL039615.

Čermák, V., Šafanda, J., Krešl, M. & Kučerová, L., 1996. Heat flow studies in Central Europe with special emphasis on data from former Czechoslovakia, *Global Tect. Metallogeny,* **5,** 109–123.

Christensen, N.I., 1996. Poisson's ratio and crustal seismology, *J. geophys. Res.,* **101,** 3139–3156.

Dahm, T. & Fischer, T., 2013. Velocity ratio variations in the source region of earthquake swarms in NW Bohemia obtained from arrival time double-differences, *Geophys. J. Int.,* **195,** 1196–1210.

Dahm, T., Fischer, T. & Hainzl, S., 2008. Mechanical intrusion models and their implications for the possibility of magma-driven swarms in NW Bohemia Region, *Stud. Geophys. Geod.,* **52**(4), 529–548.

Dreger, D.S., Tkalcic, H. & Johnston, M., 2000. Dilational processes accompanying earthquakes in the Long Valley Caldera, *Science,* **288,** 122–125.

Dudek, A., 1986. Geology and tectonic pattern of the Western Bohemia seismic area. Earthquake Swarm 1985/86 in Western Bohemia, in *Proceeding of Workshop in Mariánské Lázne,* 1986 December 1–5, Czechoslovak Academy of Science, Geoph. Institute Praha, pp. 34–37.

Eberhart-Phillips, D., 1986. Three-dimensional velocity structure in northern California Coast Ranges from inversion of local earthquake arrival times, *Bull. seism. Soc. Am.,* **76,** 1025–1052.

Eberhart-Phillips, D., 1993. Local earthquake tomography: Earthquake source regions, in *Seismic Tomography: Theory and Practice,* pp. 613–643, eds Iyer, H.M. & Hirahara, K., Chapman and Hall.

Eberhart-Phillips, D. & Michael, A.J., 1998. Seismotectonics of the Loma Prieta, California, region determined from three-dimensional Vp, Vp/Vs, and seismicity, *J. geophys. Res.,* **103,** 21 099–21 120.

Evans, J.R., Eberhart-Phillips, D. & Thurber, C.H., 1994. User's Manual for Simulps12 for Imaging Vp and Vp/Vs: a derivative of the "Thurber" tomographic inversion Simul3 for local earthquakes and explosions, Open File Rep. No. 94-431, U.S. Geological Survey, Washington, D.C.

Fischer, T., Horálek, J., Hrubcová, P., Vavryčuk, V., Bräuer, K. & Kämpf, H., 2014. Intra-continental earthquake swarms in West-Bohemia and Vogtland: a review, *Tectonophysics,* **611,** 1–27.

Geissler, W.H. *et al.*, 2005. Seismic structure and location of a CO2 source in the upper mantle of the western Eger (Ohře) Rift, central Europe, *Tectonophysics,* **24,** 1–23.

Hainzl, S., Fischer, T. & Dahm, T., 2012. Seismicity-based estimation of the driving fluid pressure in the case of swarm activity in Western Bohemia, *Geophys. J. Int.,* **191,** 271–281.

Hecht, L., Vigneresse, J.L. & Morteani, G., 1997. Constraints on the origin of zonation of the granite complexes in the Fichtelgebirge (Germany and Czech Republic): evidence from a gravity and geochemical study, *Geol. Rundschau,* **86,** 93–109.

Heinicke, J. & Koch, U., 2000. Slug flow—a possible explanation for hydrogeochemical earthquake precursors at Bad Brambach, Germany, *Pure appl. Geophys.,* **157,** 1621–1641.

Heuer, B., Geissler, W.H., Kind, R. & Kämpf, H., 2006. Seismic evidence for asthenospheric updoming beneath the western Bohemian Massif, central Europe, *Geophys. Res. Lett.,* **33,** L05311, doi:10.1029/2005GL025158.

Heuer, B., Geissler, W.H., Kind, R. & the BOHEMA working group, 2011. Receiver function search for a baby plume in the mantle transition zone beneath the Bohemian Massif, *Geophys. J. Int.,* **187,** 577–594.

Hofmann, Y., Jahr, T. & Jentzsch, G., 2003. Three-dimensional gravimetric modelling to detect the deep structure of the region Vogtland/NW-Bohemia, *J. Geodyn.,* **35,** 209–220.

Horálek, J. & Fischer, T., 2008. Role of crustal fluids in triggering the West Bohemia/Vogtland earthquake swarms: just what we know (a review), *Stud. Geophys. Geod.,* **52,** 455–478.

Horálek, J. & Šílený, J., 2013. Source mechanisms of the 2000-earthquake swarm in the West Bohemia/Vogtland region (Central Europe), *Geophys. J. Int.,* **194**(2), 979–999.

Horálek, J., Boušková, A., Hampl, F. & Fischer, T., 1996. Seismic regime of the West-Bohemian earthquake swarm region: preliminary results, *Stud. Geophys. Geod.,* **40,** 398–412.

Husen, S., Smith, R.B. & Waite, G.P., 2004. Evidence for gas and magmatic sources beneath the Yellowstone volcanic field from seismic tomographic imaging, *J. Volc. Geotherm. Res.,* **131,** 397–410.

Kämpf, H., Bräuer, K., Schumann, J., Hahne, K. & Strauch, G., 2013. CO_2 discharge in an active, non-volcanic continental rift area (Czech Republic): characterisation (δ^{13}C, ^{3}He/^{4}He) and quantification of diffuse and vent CO_2 emissions, *Chem. Geol.,* **339,** 71–83.

Kato, A., Sakai, S., Iidaka, T., Iwasaki, T. & Hirata, N., 2010. Non-volcanic seismic swarms triggered by circulating fluids and pressure fluctuations above a solidified diorite intrusion, *Geophys. Res. Lett.,* **37,** L15302, doi:10.1029/2010GL043887.

Kissling, E., 1988. Geotomography with local earthquake data, *Rev. Geophys.,* **26,** 659–698.

Kissling, E., Ellsworth, W.L., Eberhart-Phillips, D. & Kradolfer, U., 1994. Initial reference models in local earthquake tomography, *J. Geophys. Res.,* **99,** 19 635–19 646.

Kissling, E., Kradolfer, U. & Maurer, H., 1995. *VELEST User's Guide—Short Introduction,* Institute of Geophysics and Swiss Seismological Service, ETH.

Kurz, J.H., Jahr, T. & Jentzsch, G., 2003. Geodynamic modelling of the recent stress and strain field in the Vogtland/Western Bohemia swarm earthquake area using the finite-element- method, *J. Geodyn.,* **35,** 247–258.

Kurz, J.H., Jahr, T. & Jentzsch, G., 2004. Earthquake swarm examples and a look at the generation mechanism of the Vogtland/Western Bohemia earthquake swarms, *Phys. Earth planet. Inter.,* **142**(1–2), 75–88.

Lin, G. & Shearer, P.M., 2009. Evidence for waterfilled cracks in earthquake source regions, *Geophys. Res. Lett.,* **36,** L17315, doi:10.1029/2009GL039098.

Málek, J., Horálek, J. & Janský, J., 2005. One-dimensional qP-wave velocity model of the upper crust for the West Bohemia/Vogtland earthquake swarm region, *Stud. Geophys. Geod.,* **49,** 501–524.

Matte, P., Maluski, H., Rajlich, P. & Franke, W., 1990. Terrane boundaries in the Bohemian Massif: result of large-scale Variscan shearing, *Tectonophysics,* **177,** 151–170.

Mavko, G. & Mukerji, T., 1995. Seismic pore space compressibility and Gassman's relation, *Geophysics,* **60,** 1743–1749.

Mrlina, J. *et al.*, 2009. Discovery of the first Quaternary maar in the Bohemian Massif, Central Europe, based on combined geophysical and geological surveys, *J. Volc. Geotherm. Res.,* **182,** 97–112.

Muksin, U., Bauer, K. & Haberland, C., 2013. Seismic Vp and Vp/Vs structure of the geothermal area around Tarutung (North Sumatra, Indonesia) derived from local earthquake tomography, *J. Volc. Geotherm. Res.,* **260,** 27–42.

Novotný, M., Špičák, A. & Weinlich, F.H., 2013. Structural Preconditions of West Bohemia Earthquake Swarms, *Surv. Geophys.,* **34,** 491–519.

Nur, A. & Simmons, N., 1969. The effect of saturation on velocity in low porosity rocks, *Earth planet. Sci. Lett.,* **7,** 183–193.

Plomerová, J., Achauer, U., Babuška, V., Granet, M. & BOHEMA working group, 2003. Passive seismicexperiment to study lithosphere–asthenosphere system in the western partof the Bohemian Massif, *Stud. Geophys. Geod.,* **47,** 691–701.

Plomerová, J., Achauer, U., Babuška, V. & Vecsey, L., 2007. Upper mantle beneath the Eger rift (Central Europe): plume or asthenosphere upwelling?, *Geophys. J. Int.,* **169,** 675–682.

Pros, Z., Lokajíček, T., Přikryl, R., Špičák, A., Vajdová, V. & Klíma, K., 1998. Elastic parameters of West Bohemian granites under hydrostatic pressure, *Pure appl. Geophys.,* **151,** 631–646.

Růžek, B. & Horálek, J., 2013. Three-dimensional seismic velocity model of the West Bohemia/Vogtland seismoactive region, *Geophys. J. Int.,* **195,** 1251–1266.

Špičak, A. & Horálek, J., 2001. Possible role of fluids in the process of earthquake swarm generation in the West Bohemia/Vogtland seismoactive region, *Tectonophysics,* **336,** 151–161.

Stammler, K., 1993. Seismichandler programmable multichannel data handler for interactive and automatic processing of seismological analyses, *Comput. Geosci.,* **19,** 135–140.

Švancara, J., Gnojek, I., Hubatka, F. & Dědáček, K., 2000. Geophysical field pattern in the West Bohemian geodynamic active area, *Stud. Geophys. Geod.,* **44,** 307–326.

Švancara, J., Havíř, J. & Conrad, W., 2008. Derived gravity field of the seismogenic upper crust of SE Germany and West Bohemia and its comparison with seismicity, *Stud. Geophys. Geod.,* **52,** 567–588.

Takei, Y., 2002. Effect of pore geometry on Vp/Vs: from equilibrium geometry to crack, *J. geophys. Res.,* **107,** doi:10.1029/2001JB000522.

Thurber, C.H. & Eberhart-Phillips, D., 1999. Local earthquake tomography with flexible gridding, *Comput. Geosci.,* **25,** 809–818.

Thurber, C.H., 1983. Earthquake locations and three-dimensional crustal structure in the Coyote Lake area, central California, *J. geophys. Res.,* **88,** 8226–8236.

Thurber, C.H., 1993. Local earthquake tomography: velocities and Vp/Vs – theory, in *Seismic Tomography: Theory and Practice,* pp. 563–583, eds Iyer, H.M. & Hirahara, K., Chapman and Hall.

Toomey, D.R. & Foulger, G.R., 1989. Tomographic inversion of local earthquake data from the Hengill-Grensdalur Central Volcano Complex, Iceland, *J. geophys. Res.,* **94,** 17 497–17 510.

Um, J. & Thurber, C.H., 1987. A fast algorithm for two-point seismic ray tracing, *Bull. seism. Soc. Am.,* **77,** 972–986.

Vavryčuk, V., Bouchaala, F. & Fischer, T., 2013. High-resolution fault image from accurate locations and focal mechanisms of the 2008 swarm earthquakes in West Bohemia, Czech Republic, *Tectonophysics,* **590,** 189–195.

Vidale, J.E. & Shearer, P.M., 2006. A survey of 71 earthquake bursts across southern California: exploring the role of pore fluid pressure fluctuations and aseismic slip as drivers, *J. geophys. Res.,* **111**(B5), doi:10.1029/2005JB004034.

Wagner, G.A., Gögen, K., Jonckheere, R., Wagner, I. & Woda, C., 2002. Dating of Quaternary volcanoes Komorni Hůrka (Kammerbühl) and Železna Hůrka (Eisenbühl), Czech Republic, by TL, ESR, alpha-recoil and fission track chronometry, *Z. geol. Wiss.,* **30**(3), 191–200.

Weinlich, F.H., Tesař, J., Weise, S.M., Bräuer, K. & Kämpf, H., 1998. Gas flux distribution in mineral springs and tectonic structure in the western Eger Rift, *J. Czech Geol. Soc.,* **43**(1–2), 91–110.

Weise, S., Brauer, K., Kämpf, H., Strauch, G. & Koch, U., 2001. Transport of mantle volatiles through the crust tracen by seismically released fluids: a natural experiment in the earthquake swarm area Vogtland/NW Bohemia, Central Europe, *Tectonophysics,* **336,** 137–150.

Wilde-Piórko, M. *et al.*, 2008. PASSEQ2006–2008: passive seismic experiment in Trans-European Suture Zone, *Stud. Geophys. Geod.,* **52,** 439–448.

Zhang, H. & Thurber, C.H., 2003. Double-difference tomography: the method and its application to the Hayward fault, California, *Bull. seism. Soc. Am.,* **93,** 1175–1189.

Ziegler, P.A., 1992. European Cenozoic rift system, *Tectonophysics,* **208,** 91–111.

Zulauf, G., Bues, C., Dörr, W. & Vejnar, Z., 2002. 10 km minimum throw along the West Bohemian shear zone: evidence from dramatic crustal thickening and high topography in the Bohemian Massif (European Variscides), *Int. J. Earth Sci.,* **91,** 850–864.